Molecular Therapy
Oncolytics
Original Article

Cancer imaging and therapy utilizing a novel NIS-expressing adenovirus: The role of adenovirus death protein deletion

Matthew Glen Robertson,[1] Benjamin Bruce Eidenschink,[1,2] Eriko Iguchi,[3,4] Stanislav O. Zakharkin,[5] Christopher J. LaRocca,[1] Ezequiel J. Tolosa,[3] Mark J. Truty,[6] Kari Jacobsen,[1] Martin E. Fernandez-Zapico,[3] and Julia Davydova[1,7]

[1]Department of Surgery, University of Minnesota, Minneapolis, MN 55455, USA; [2]School of Medicine, University of Missouri at Kansas City, MO 64110, USA; [3]Schulze Center for Novel Therapeutics, Division of Oncology Research, Mayo Clinic, Rochester, MN 55905, USA; [4]Department of Gastroenterology and Hepatology, Graduate School of Medicine, Kyoto University, Kyoto, Japan; [5]WebMD, New York, NY 10014, USA; [6]Department of Surgery, Mayo Clinic, Rochester, MN 55905, USA; [7]Masonic Cancer Center, University of Minnesota, Minneapolis, MN 55455, USA

Encoding the sodium iodide symporter (NIS) by an adenovirus (Ad) is a promising strategy to facilitate non-invasive imaging and radiotherapy of pancreatic cancer. However, insufficient levels of NIS expression in tumor cells have limited its clinical translation. To optimize Ad-based radiotherapy and imaging, we investigated the effect of Ad death protein (ADP) deletion on NIS expression. We cloned two sets of oncolytic NIS-expressing Ads that differed only in the presence or absence of ADP. We found that ADP expression negatively affected NIS membrane localization and inhibited radiotracer uptake. ADP deletion significantly improved NIS-based imaging in pancreatic cancer models including patient-derived xenografts, where effective imaging was possible for up to 6 weeks after a single virus injection. This study demonstrates that improved oncolysis may hinder the therapeutic effect of oncolytic viruses designed to express NIS. *In vivo* studies in combination with ^{131}I showed potential for effective radiotherapy. This also highlights the need for further investigation into optimal timing of ^{131}I administration and suggests that repeated doses of ^{131}I should be considered to improve efficacy in clinical trials. We conclude that ADP deletion is essential for effective NIS-based theranostics in cancer.

INTRODUCTION

Oncolytic viral therapy continues to grow in importance as a cancer therapeutic strategy. In addition to direct cytolysis of tumor cells as part of viral replication and induction of tumor-specific immune responses, oncolytic viruses are also able to deliver transgenes to tumor cells. Early clinical trials with oncolytic viruses as single-agent therapies proved to be poorly effective. Consequently, inclusion of transgenes to selectively express therapeutic proteins has developed to increase the effectiveness of virotherapy.

The sodium iodide symporter (NIS) has become a popular candidate protein for insertion into oncolytic viruses.[1] NIS is a native transmembrane glycoprotein primarily expressed in the thyroid that mediates iodine uptake. For many years, clinicians have exploited the function and limited native expression of NIS to facilitate radioiodine uptake, providing a unique imaging and treatment strategy for thyroid cancer.[2] Not surprisingly, the idea to deliver NIS to other cancers using viral vectors has been extensively explored over the last decade, mainly for use as an adjunct cancer-imaging tool.[1] Indeed, virus-mediated tumor expression of NIS can enable non-invasive tumor visualization through the use of standard SPECT/computed tomography (CT) or PET/CT imaging with commercially available radiotracers. This approach to deliver NIS for cancer imaging has been undertaken with many viral vectors, including adenovirus (Ad), measles, vaccinia, herpes simplex, poxvirus, and vesicular-stomatitis viruses.[1,3–10]

Over the last few years, our lab has designed oncolytic Ad (OAd) vectors that encode therapeutic proteins in the adenoviral E3 region (E3), which we refer to as the ΔE3 system.[11–20] Many native genes from E3 are neither requisite for Ad infection or replication, and thus they can be deleted to provide space for transgenes while still preserving genome size and replication competence. Because transgene expression from E3 is controlled by the Ad major late promoter, therapeutic proteins are produced with each round of virus replication.[11,15] In addition, we have shown that non-invasive detection of E3 transgenes can serve as a surrogate measure of virus replication to inform therapeutic potential.[11]

An important component of E3 is the Ad death protein (ADP), which promotes host cell membrane degradation to allow release of viral progeny.[21,22] In our prior studies, we confirmed that deletion of the l2.5K,

Received 16 December 2020; accepted 1 March 2021;
https://doi.org/10.1016/j.omto.2021.03.002.

Correspondence: Matthew Glen Robertson, Department of Surgery, University of Minnesota, Minneapolis, MN 55455, USA.
E-mail: robe1414@umn.edu

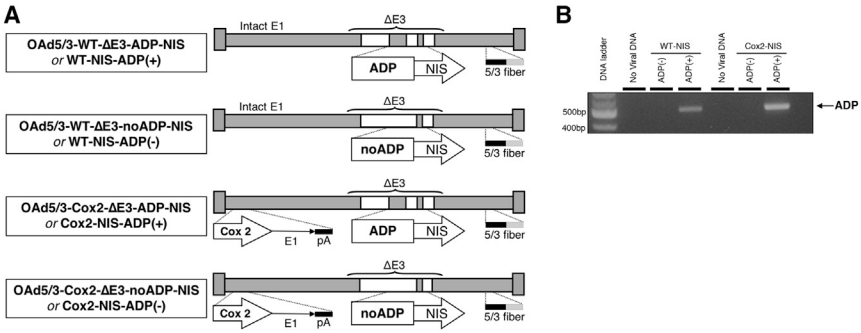

Figure 1. Viral constructs

(A) Schematic representation of OAd-NIS vectors. Constructs are based on adenovirus type 5 (Ad5) and include deletion of the 12.5K, 6.7K, gp19K, RID-α, RID-β, and 14.7K genes from the E3 region. The ADP gene was removed from ADP^{-} vectors. The vectors are equipped with the Ad5/Ad3-modified fiber to overcome coxsackie Ad receptor (CAR) deficiency and a Cox2 promoter to restrict replication and gene expression to permissive tumors. (B) PCR verification of ADP presence or absence in each vector.

6.7K, gp19K, RID-α and RID-β, and 14.7K genes, while maintaining ADP in the E3 region, results in overexpression of ADP and subsequent improvement in oncolysis.[11] Subsequently, we have utilized our ΔE3 system to express various imaging and therapeutic transgenes (e.g., EGFP, RFP, luciferase, interferons, and NIS) in different tumor types.[11,12,15] All of these constructs, including NIS-expressing OAds (OAd-NIS), were designed to overexpress ADP to improve virus spread and oncolysis in solid tumors. First generation ADP-positive (ADP(+)) OAd-NIS vectors demonstrated effective oncolysis and were able to mediate radioisotope uptake in prostate and lung cancer models.[13,14,19] However, we were concerned that ADP may have deleterious effects on the membrane localization and functionality of NIS.

Here, we investigated the effect of ADP deletion on NIS expression and subsequent radiotracer uptake with the goal to improve NIS-based cancer therapy and imaging, focusing on pancreatic cancer. For this purpose, we cloned two sets of ΔE3-based OAd vectors expressing NIS from the E3 region that differ only in the presence or absence of ADP. Additional genetic modifications included utilization of a chimeric Ad5/Ad3 fiber to improve virus infectivity for coxsackie and Ad receptor (CAR)-deficient pancreatic ductal adenocarcinoma (PDAC) tumors and the cyclooxygenase-2 (Cox2) promoter to drive tumor-selective replication.[17,23,24] We compared NIS expression and radioiodine uptake *in vitro* and *ex vivo* and assessed virus-mediated *in vivo* imaging. We found that ADP deletion significantly improved NIS expression from E3, which resulted in improved imaging capabilities. We have also confirmed the feasibility of using our OAd-NIS vectors to facilitate radiotherapy with ^{131}I.

RESULTS

NIS-expressing Ad structure

Four NIS-expressing Ad vectors were constructed resulting in two pairs of ADP(+) and ADP-negative (ADP(−)) replication-competent OAds with either wild-type (WT) or Cox2-controlled replication (Figure 1A). The ADP gene was removed from ADP(−) vectors, while identical ADP(+) counterparts retained ADP in the E3 region. ADP status was confirmed using qPCR (Figure 1B).

Deletion of ADP does not affect the killing ability of OAd-NIS

The replication abilities and oncolytic potentials of NIS-expressing adenoviral vectors were evaluated *in vitro* with a crystal violet assay. The cancer cells were infected at a low titer of 1 viral particle (vp)/cell to allow at least a few rounds of virus replication (Figure 2A). At this low titer, ADP(−) viruses were slower to kill cells than their identical ADP(+) counterparts; however, their killing ability was similar to ADP(+) at later time points or upon higher viral titers (data not shown). Uniformly, vectors with Cox2-regulated replication were less efficient at oncolysis than their WT-replication counterparts, but because these vectors also use the chimeric Ad5/3 fiber, their oncolytic potential remained comparable to Ad5WT. Importantly, Cox2-controlled viruses demonstrated insignificant viral spread in Cox2^{-} BT474 cells, indicating the feasibility of the Cox2 promoter to restrict novel OAd-NIS virus replication to Cox-2^{+} cells consistent with our previous findings.[17,23]

To better quantify virus-induced cytolysis, we analyzed A549 and Panc-1 cell viability at low-titer infection using a cell proliferation assay (Figure 2B). Both ADP(+) and ADP(−) viruses produced a statistically significant ($p < 0.05$) decrease in cell viability compared to untreated controls. ADP(−) viruses were slower to kill than their ADP(+) counterparts (day 14 post-infection [p.i.] versus day 7 p.i.). These experiments demonstrate that despite being less efficient than ADP(+) counterparts in killing cancer cells *in vitro*, ADP-deleted viruses still achieve an appropriate oncolytic effect by the end of the experiment.

The Cox2 promoter selectively limits OAd-NIS replication and radioiodine uptake *ex vivo* in human pancreatic cancer tissue slices

We tested the selectivity of NIS-expressing vectors through *ex vivo* infection of human pancreatic tumors and adjacent normal pancreatic tissues (Figure 3A). Viral copy numbers in tissues infected with the Cox2 promoter-controlled virus (Cox2-NIS) were seven orders of magnitude higher in tumor compared to normal pancreas (7×10^{3} versus 2×10^{-4}, respectively; Figure 3B). In contrast, WT-replication counterpart (WT-NIS)-infected tissues showed similar levels of virus replication in tumor and normal pancreas (1×10^{4} versus 1×10^{3}, respectively). Of note, viral copies of Cox2-NIS and WT-NIS in pancreatic tumor tissues were nearly equivalent (7×10^{3} versus 1×10^{4}, respectively) in this preclinical model. Similarly, radioactivity after Cox2-NIS

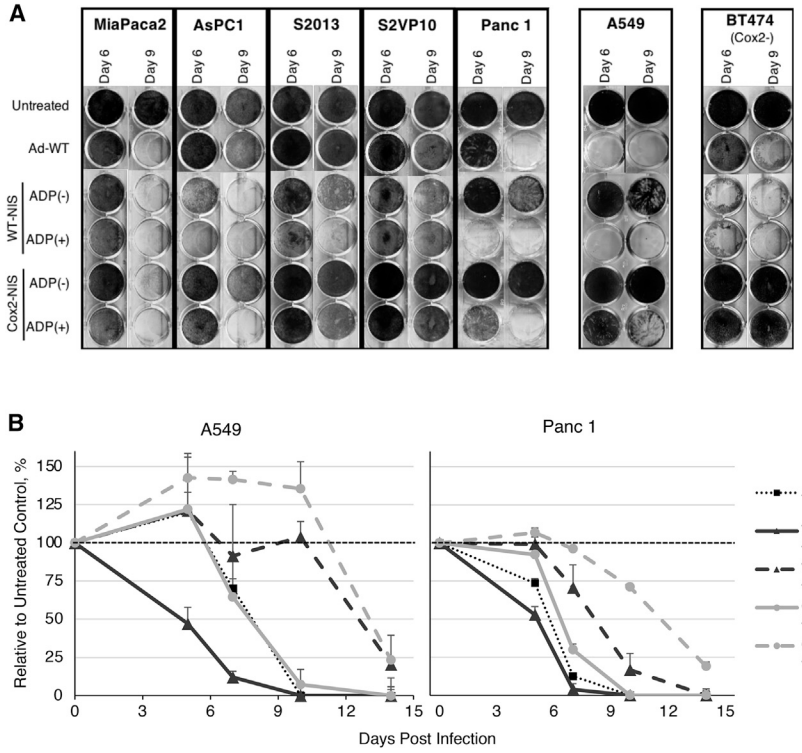

Figure 2. Oncolytic potential of OAd-NIS vectors

(A) Crystal violet staining of pancreatic cancer and Cox2^{-} BT474 cells. The human A549 lung carcinoma cell line was used as standard CAR-, Ad3-receptor-, and Cox2^{+} control. Wild-type Ad5 virus (Ad5WT) was used as a positive control to evaluate the cytolytic potential of recombinant vectors. The oncolytic effect of 5/3 fiber-modified, Cox2-controlled vectors was comparable to that of Ad5Wt. Staining of Cox2^{-} BT474 cells shows susceptibility to WT viruses but resistance to Cox2-controlled viruses. (B) Cell viability MTS assay of A549 and Panc1 cells. Error bars represent standard deviation. All viruses were able to eliminate all tumor cells; however, ADP(–) viruses killed cells more slowly than ADP(+) viruses.

infection was significantly higher in tumors compared to normal tissue while iodine uptake in WT-NIS-infected tissues was not statistically different (Figure 3C).

ADP deletion improves NIS expression *in vitro*

To understand the impact of ADP on NIS expression, we performed immunofluorescent analyses and fluorescence-activated cell sorting (FACS) analyses of A549 cells infected with ADP(+) and ADP(–) vectors (Figures 4A and 4B). NIS expression was observed after infection with all NIS-expressing viruses, with significantly higher levels of NIS at later time points indicating replication-dependent expansion of gene expression. Immunostained cells clearly showed potentiated NIS expression with ADP(–) vectors compared to ADP(+) counterparts. These data correlated well with FACS analysis. Importantly, the ADP(–) Cox2-NIS-ADP(–) demonstrated clearly improved localization of NIS in cellular membrane when compared to its ADP(+) counterpart (Figures 4C and 4D). Overall, these analyses revealed higher levels of NIS expression and improved membrane localization of NIS after infection with ADP-deleted viruses.

Feasibility of radioiodine therapy with NIS-expressing Ad vectors

The ability of OAd-NIS to facilitate radiotherapy *in vivo* was evaluated in A549 subcutaneous tumors in mice (Figure 5A). Both oncolytic Cox2-NIS viruses (ADP(+) and ADP(–)) in combination with radioactive iodine (^{131}I) showed statistically significant tumor reduction compared to the untreated control while the therapeutic effect of AdCMV-NIS combined with ^{131}I was not significantly different. We also compared the growth curves of virus monotherapy versus combination therapies. While all viruses trended toward further restriction of tumor growth after combination with ^{131}I therapy (compared to monotherapy groups), only the Cox2-NIS-ADP(+) treatment group reached statistical significance. Combination therapy with Cox2-NIS-ADP(+) was the most efficacious treatment regimen at killing tumor in this experiment. However, comparison of combination therapy with Cox2-NIS-ADP(–) versus Cox2-NIS-ADP(+) revealed no significant difference between these two groups.

11 and 19 days post treatment with Ad (8 and 16 days after I^{-131} administration), tumors and uninvolved leg muscle were measured for radioactivity using a gamma counter and tumor radioactivity was expressed relative to muscle (Figure 5B). Here we found correlation with the previous *in vitro* studies (Figure 4), with Cox2-NIS-ADP(–) outperforming its ADP(+) counterpart and AdCMV-NIS control. Cox2-NIS-ADP(–) infection resulted in radioactivity that was 2 times higher than PBS control (5.0 and 2.6, respectively). Tumors injected with Cox2-NIS-ADP(+) and AdCMV-NIS had radioactivity that was above control levels but lower than Cox2-NIS-ADP(–)-injected tumors (3.1 and 3.7, respectively). Radioactivity measurements had large variation between animals and consequently, the uptake differences did not achieve statistical significance. By day 19 p.i., the counts per minute (CPM) counts in tumors were not different from uninvolved leg muscles (data not shown). The nonsignificant differences in radiotracer uptake at day 11 and lack of radiotracer at day 19 could be due to complete clearance of ^{131}I from the body, including tumors. These findings suggest that a single dose of ^{131}I is likely insufficient to capitalize on the high levels and extended duration of Ad-mediated NIS expression. Furthermore, the absence of iodine at later time points could explain the limited therapeutic effect of the combination therapy with ^{131}I.

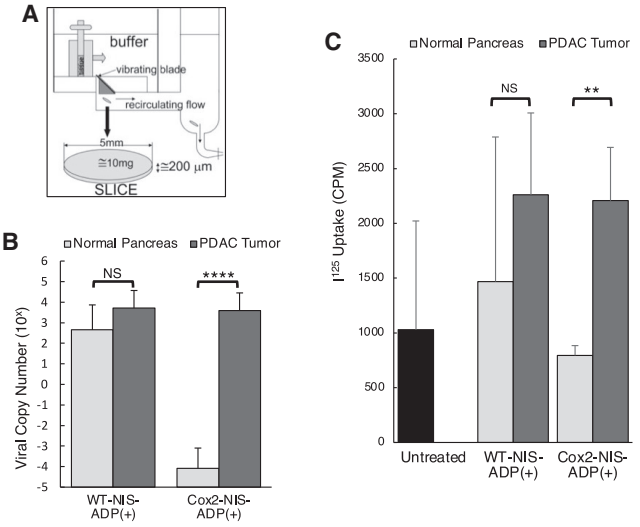

Figure 3. *Ex vivo* selective replication and iodine uptake in human pancreatic tissue slices

(A) Schematic of tissue slicer used in experiments. (B) Normal human pancreatic tissues and human pancreatic tumors were infected *ex vivo* and viral copy numbers determined by RT-PCR. Error bars represent standard error. There was no statistical difference between WT viral replication in normal pancreas and tumor tissues, while the Cox2 promoter restricted replication to tumor with significantly less replication in normal pancreas compared to tumor. (C) Human normal and cancerous PDAC tissues were infected *ex vivo* and incubated with ^{125}I, and radioactivity was measured. The untreated bar represents a combination of untreated normal and tumor tissues. Error bars represent standard deviation. Cox2-controlled NIS vector showed no replication in normal pancreas (below untreated control) and robust replication in adenocarcinoma comparable to that with the non-selective (WT replication) counterpart. (*$p < 0.05$; **$p < 0.01$; NS, not significant).

ADP deletion enhances *in vivo* imaging capability of NIS-expressing vectors

The *in vivo* imaging potential of ADP(+) and ADP(−) NIS-expressing vectors was first compared in nude mice with human pancreatic cancer Panc1 xenografts. Two different doses of adenoviral vectors (high: 4×10^{10} and low: 4×10^{9} viral particles) were analyzed, with the lower dose being used to avoid a rapid virus-killing effect, to ensure radiotracer uptake could be evaluated (Figure 6A). At both dosing levels, SPECT/CT images showed much higher radiotracer uptake with Cox2-NIS-ADP(−) when compared to its ADP(+) counterpart and control vectors (WT-NIS-ADP(+) and AdCMV-NIS, a positive control employed in human clinical trials of NIS-mediated gene therapy for prostate cancer). In addition to improved uptake at each sampling, Cox2-NIS-ADP(−) facilitated tumor-specific ^{99m}Tc uptake 4 weeks after a single virus injection compared to 1 week with AdCMV-NIS. The long duration of imaging capability indicates that NIS is being expressed in a replication-dependent manner, allowing for continued NIS production as the virus spreads throughout the tumor. In contrast, AdCMV-NIS is replication-deficient and thus unable to sustain NIS expression for extended periods of time. The functional advantage of replication-dependent gene expression for imaging is clearly visible in the results of this experiment.

Notably, while ADP deletion did not affect the spread of virus in solid tumors as shown by Ad-hexon staining, it did result in higher levels of NIS expression that remained robust for at least 4 weeks p.i. (Figure 6B). This accounts for the excellent duration of imaging capability of Cox2-NIS-ADP(−).

The therapeutic potential of the NIS-expressing vectors as monotherapies was also evaluated with two different viral doses (Figure 6C). All replication-competent NIS viruses showed statistically significant tumor reduction compared with untreated controls at both high and low viral titers. Of note, Cox2-NIS-ADP(+) and Cox2-NIS-ADP(−) were not statistically different at slowing tumor growth. The slower oncolysis with ADP(−) vectors seen *in vitro* did not appear to hamper the virus's ability to control tumor growth *in vivo*. Overall, these data suggest that deletion of ADP has clear positive effects on the imaging capability of these OAd-NIS vectors and does not reduce their antitumor activity, compared to viruses expressing ADP.

ADP deletion improves NIS expression and subsequent imaging in PDAC patient-derived xenografts

Virus-mediated SPECT/CT imaging was next analyzed in PDAC patient-derived xenografts (PDXs). Similar to human disease, the human-biopsy-proven PDAC tissues (Figure S1) exhibited varied tumor growth rates leading to different lengths of time to reach euthanasia criteria and heterogeneous responses to virus treatment as measured by radiotracer uptake. To objectively evaluate viral effects across the heterogeneous PDX cohorts, after each imaging session, we quantified radiotracer uptake from the tumor of each mouse and compared it against an area of uninvolved muscle. This provided a relative difference (RD) in uptake between tumor and muscle for each animal at each time point, allowing for comparison across cohorts (Figure 7A). This analysis suggested significant improvement in radiotracer uptake in tumors injected with Cox2-NIS-ADP(−) compared with both Cox2-NIS-ADP(+) and AdCMV-NIS. Again, we observed excellent duration of imaging with ADP(−) that facilitated radiotracer uptake for up to 6 weeks after only a single viral injection. Illustrative images from two PDAC PDX cohorts (patients #177 and #27) are shown in Figure 7B.

We sought to characterize the PDX model and analyze viral spread and activity within patient tumors using immunohistochemical methods. Figure 7C shows sequential slices of a PDX infected with Cox2-NIS-ADP(−). Hematoxylin and eosin (H&E) staining shows evidence of cellular debris consistent with oncolysis (Figure 7C, image i). Collagen staining revealed a highly desmoplastic tumor, accurately reflecting the known microenvironment of human pancreatic cancer (Figure 7C, image ii). Immunohistochemistry (IHC) staining for Ad-hexon, NIS, and CYK19 (a marker of pancreatic ductal cells) show active adenoviral infection of pancreatic ductal cells within the tumor and virus-mediated NIS expression (Figure 7C, images iii–v). Active adenoviral infection as evidenced by Ad-hexon and NIS expression were present in tumors injected with either ADP(+) and ADP(−) viruses (Figure 7D). Ad-hexon expression quantified by ImageJ showed no statistical difference between the two tumor samples; however, NIS

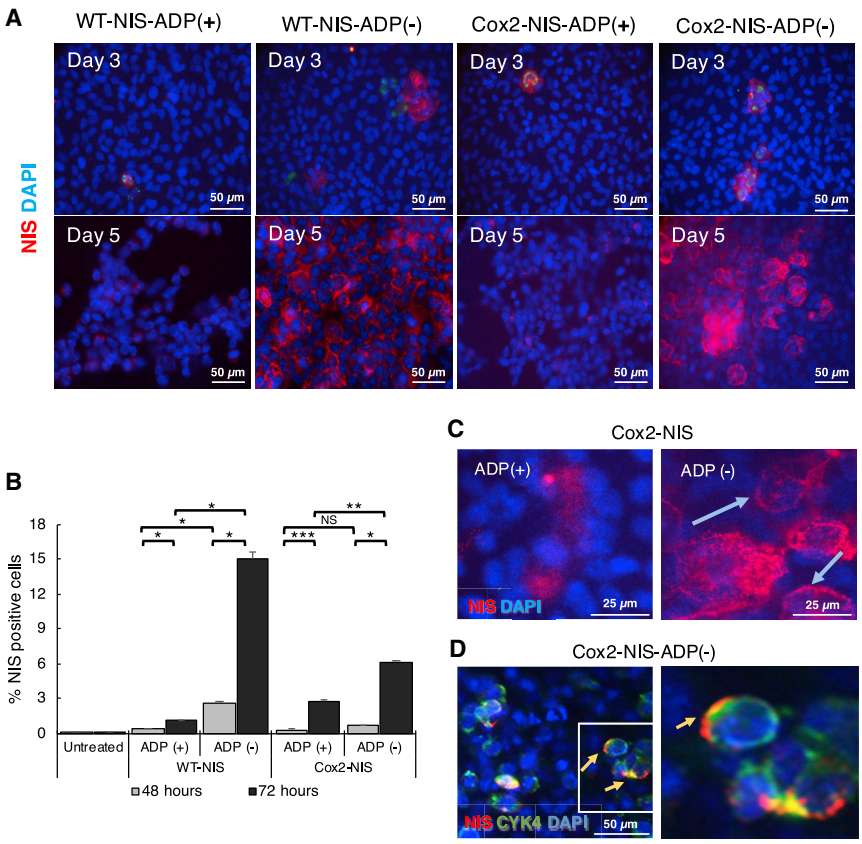

Figure 4. ADP deletion improves NIS expression and membrane localization

(A) A549 cells were incubated at 10 vp/cell for 3 and 5 days. Immunostaining showed replication-dependent NIS expression (red) increased from day 3 to 5 and improved NIS levels with ADP(–) constructs. (B) A549 cells infected with NIS-expressing vectors were analyzed by FACS with NIS antibodies. Error bars represent standard deviation. Each virus showed a significant increase in NIS expression at 72 h compared to 48 h p.i. ADP(–) produced higher NIS expression compared with ADP(+) (*$p < 0.05$; **$p < 0.01$; ***$p < 0.001$; NS, not significant). (C) A549 cells were infected with ADP(+) and ADP(–) viruses at 10 vp/cell and incubated for 5 days. Immunostaining images for NIS showed better membrane localization of NIS after infection with ADP(–). (D) To confirm NIS membrane localization, we co-stained Cox2-NIS-ADP(–)-infected cells with NIS (red) and membrane protein CYK4 (green). Colocalization is shown as yellow.

expression was about 10-fold higher in tumors infected with Cox2-NIS-ADP(–) (Figure 7E).

We also measured tumor growth for PDX mice and plotted this data by treatment group (Figure 7F). As was seen with Panc1 xenografted mice, we observed a significant reduction in tumor growth upon injection of any NIS-expressing virus. No statistical difference was seen between the tumor burden of ADP(+)- and ADP(–)-injected mice. All these data confirm active Ad infection and virus-induced NIS expression in human tumors infected with Cox2-NIS-ADP(–). Additionally, the data provide further support of Cox2-NIS-ADP(–) as a superior vector due to improved NIS expression leading to better imaging potential while also providing similar tumor control to Cox2-NIS-ADP(+).

DISCUSSION

For many decades, cancer treatment has benefitted from a multimodal approach that historically has included some combination of surgery, chemotherapy, and radiation with more recent additions of targeted biologics and immunotherapies. Oncolytic viruses designed to express the dual-function gene NIS offer the potential of a single theranostic agent that provides multiple clinical benefits including assisting in diagnosis and prognostication through improved cancer imaging, as well as combining direct oncolysis, tumor specific sensitization of host immunity, and radiotherapy.[25] With such promise, we must ask why these viruses have thus far seen little use as theranostic agents. Indeed, while many NIS-expressing viruses have been reported as potential imaging tools in preclinical studies, few have been investigated for their ability to facilitate NIS-based radiotherapy.[1,2] Overall, the clinical translation of NIS-based imaging and radiotherapy remains a challenge and early clinical trials have focused mainly on monitoring virus spread.[26–29] These studies have highlighted the difficulties in achieving sufficient NIS expression to support clinically relevant radioiodine uptake in tumors.

The goal of this work was to remedy the problem of low NIS levels by optimizing the vectors to maximize NIS expression. In addition to NIS expression through the partially deleted E3 region, we utilized two previously established strategies to improve infectivity and selectivity in solid tumors including pancreatic adenocarcinoma.[17,18,23,24] A chimeric fiber protein (Ad5/3) was used to promote virus infectivity in tumors by retargeting the virus to CD46 and desmoglein 2 receptors to overcome CAR deficiency on the surface of tumor cells. We also used the Cox2 promoter to drive Ad replication, limiting NIS expression and viral spread to $Cox2^+$ tumors. These strategies functioned well in preclinical models where virus replication and NIS expression were effectively restricted to pancreatic tumors.

We chose to utilize our partial ΔE3 vector design because it achieves high levels of transgene expression and allows for monitoring of Ad replication. We were specifically interested in exploring the effect of the ADP on NIS expression from E3. More than a decade ago, Dornonin et al.[21] demonstrated that deletion of non-essential E3 region genes while maintaining ADP resulted in higher levels of ADP expression and subsequently increased cytopathic effect. Since then, ADP-overexpressing vectors have been used by many, including us, with the goal to

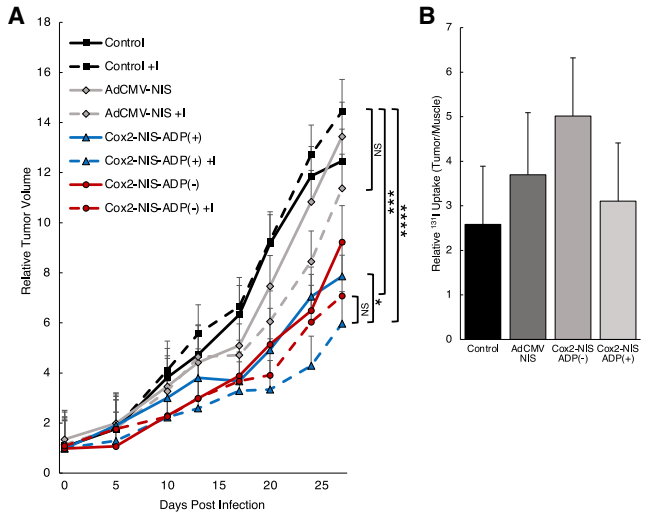

Figure 5. Combination with ^{131}I improved therapeutic effect of virotherapy

(A) A549-bearing mice were treated with a single Ad injection alone or in combination with ^{131}I (administrated 3 days p.i.). Two groups served as controls (PBS alone and PBS plus ^{131}I). Both Cox2-NIS-ADP(+)and Cox2-NIS-ADP(–) in combination with ^{131}I reduced tumor burden compared to PBS plus ^{131}I. Combination therapies improved tumor control over virus alone (*$p < 0.05$; ***$p < 0.001$; ****$p < 0.0001$; NS, not significant). (B) On day 11 p.i., radioactivity measured in tumor and uninvolved muscle and presented as relative ^{131}I uptake (tumor CPM/muscle CPM). Cox2-NIS-ADP(–) trended toward higher radioiodine uptake over control. Error bars represent standard error.

improve the oncolytic potential of Ad-based therapeutics. However, for OAd-ΔE3-NIS vectors, our goal is not simply oncolysis, but also effective NIS expression, which we have now shown is enhanced by deletion of ADP. This work is the first to highlight the impacts of adenoviral ADP on NIS-facilitated radiotherapy and imaging. Our data suggest that ADP expression negatively affects NIS membrane localization thereby inhibiting radiotracer uptake. Moreover, ADP deletion improves transmembrane localization of NIS and allows the host cells to remain alive through more replication cycles, thus producing more functional NIS that can mediate radiotherapy and effective imaging in cancer. We have shown that ADP deletion significantly improves NIS-based imaging in different preclinical models including PDAC PDXs, thereby facilitating effective imaging for more than 6 weeks after only a single virus injection. Our experiments were performed with human tumors to assess replication-dependent NIS expression and killing ability of the oncolytic Ad; however, further investigations using immunocompetent models (e.g., Syrian hamsters) will be required to elucidate the host-virus interactions of our specific viral vector.

Effective radiotherapy facilitated by NIS-expressing oncolytic viruses continues to be difficult to achieve. Our radiotherapy experiment confirmed the possibility of OAd-ΔE3-NIS-mediated radiotherapy and paves the way to achieving true clinical benefit. Our imaging studies, in which technetium was administered each time immediately before SPECT/CT imaging, clearly show radiotracer uptake and vivid imaging in tumors for 4–6 weeks after a single injection of OAd-ΔE3-NIS. However, our radiotherapy experiments measured radiotherapy uptake 8 and 16 days after ^{131}I injection and revealed lower uptake than would be expected based on hypothesized NIS levels extrapolated from *in vitro* and imaging experiments. Unlike thyroid tissue, which retains iodine in the cell by incorporating it into thyroid hormone, tumors lack this organification process and consequently ^{131}I leaks out of tumor cells and is excreted.[25] Once the initial ^{131}I injection has been cleared from circulation, NIS expression can have no further therapeutic effect. We conclude that the limited improvement of combination therapy with ^{131}I over virus monotherapy is due to the lack of circulating ^{131}I for much of the duration of the experiment, and most of the observed restriction of tumor growth over the 27-day experiment was due to viral activity alone. Hence, we anticipate that repeated injections of ^{131}I will be required for effective tumor destruction. Additionally, we anticipate that because of the heterogeneity seen in all cancers, the timing and dosage of ^{131}I will vary and should be determined using non-invasive imaging techniques to verify adequate NIS expression. Standard dosimetry calculations based on radiotracer uptake seen by SPECT/CT imaging could provide a reasonable estimate of NIS activity in individual tumors and guide the start date and dosing of ^{131}I therapy for maximal effect with minimal toxicity. The combination of non-invasive imaging with radiotherapy will likely prove to be a key component of effective oncolytic virus-mediated radiotherapy.

In conclusion, this study demonstrates that, counterintuitively, improving oncolysis may actually hinder the therapeutic effect of oncolytic viruses designed to express the NIS protein. By identifying the importance of ADP deletion to optimize functional NIS expression from the Ad E3 region, we have demonstrated the feasibility of radiotherapy and the superior imaging capabilities that can be achieved with NIS-expressing Ad in human pancreatic cancer models. Our findings also emphasize the importance of the timing of iodine administration to achieve clinically relevant results. We hope that this work will provide additional knowledge that can be applied in the design of future oncolytic viruses to facilitate NIS-based radiotherapy and imaging. Virus-mediated oncolysis combined with targeted ^{131}I radiotherapy and improved imaging to both guide and monitor therapy has great potential to be transformative for devastating cancers such as pancreatic adenocarcinoma.

MATERIALS AND METHODS

Cell lines

The human PDAC Panc-1, ASPC1, MiaPaca2, lung carcinoma A549, and breast cancer BT474 cell lines were obtained from American Type Culture Collection. S2013 and S2VP10 cell lines representing the aggressive metastatic forms of PDAC were a generous gift from Dr. Selwyn Vickers.[30,31] The cells were grown in DMEM supplemented with 1% penicillin streptomycin, 2 mM L-glutamine, and 5% fetal bovine serum (20% for ASPC1). BT474 was cultured in RPMI medium supplemented with 15% PBS and bovine insulin (0.01 mg/mL).

Adenoviral vectors

Two pairs of NIS-expressing ADP(+) and ADP(–) replication-competent OAds with WT and Cox2-controlled replication were

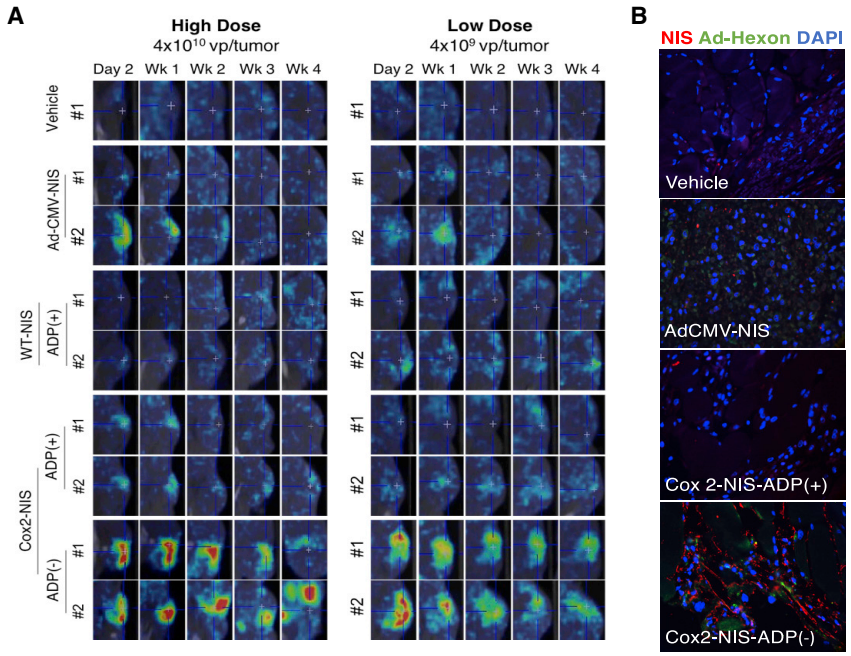

Figure 6. OAd-NIS imaging and tumor control in human Panc 1 xenografts

(A) Representative images of SPECT/CT with ^{99m}Tc in Panc1 xenografts demonstrating superiority of imaging facilitated by Cox2-NIS-ADP(–). A replication-deficient AdCMV-NIS (employed in a phase I clinical trial for prostate cancer) and a WT replication WT-NIS-ADP(+) were used as control vectors. (B) Histologic sections from tumors 28 days after low dose infection stained for NIS and Ad-hexon showing improved NIS expression after Cox2-NIS-ADP(–) (20× magnification). (C) Xenograft growth curves. Error bars represent standard deviation. All virus-injected tumors were significantly smaller than control after both high and low titer injections ($p < 0.01$ for all comparisons). Tumor growth after Cox2-NIS-ADP(+) and Cox2-NIS-ADP(–) injection were statistically equivalent (high dose: $p = 0.971$; low dose: $p = 0.571$).

constructed based on the previously reported E3 system. Briefly, the E3 3.6K and 7.5K genes were maintained while non-essential 6.7K, gp19K, RID-α, and -β, 14.7K were deleted.[11,15,16] The initiating ATG codon of the 12.5 gene was inactivated by replacement with TTA.[15] The ADP gene was removed from ADP(–) vectors, while identical ADP(+) counterparts retained ADP in the E3 region. The viruses were propagated in A549 cells, purified by cesium-chloride gradient ultracentrifugation, and dialyzed in PBS with 10% glycerol. Titration was performed with a plaque-forming unit (PFU) assay and optical density-based measurements.[32] The vp/PFU ratios for these vectors were in the range of 10–80. Purified virions were confirmed by qPCR to contain the Cox2 promoter, 5/3 fiber, NIS, and ADP. As a control vector, replication-deficient AdCMV-NIS employed in the phase I clinical trial of NIS-based therapy for men with prostate cancer (ClinicalTrials.gov: NCT00788307) was used.[3]

Crystal violet assay

2.5×10^4 cells per well were plated in 12-well plates and infected at 1–10 vp/cell in 200 μL of appropriate medium. 3 h p.i., medium was replaced and incubated up to 12 days. Medium was aspirated and cells fixed with 10% buffered formalin followed with 1% crystal violet staining.[23]

Cell viability assay

3,000 cells per well were plated in 96-well plates and infected at 10 vp/cell in 100 μL of appropriate medium. On the next day, 100 μL of the growth medium containing 1% FBS was added. The cells were incubated for 5–12 days and the number of viable cells was determined using the Cell Titer 96 Aqueous Cell Proliferation Assay as instructed by the manufacturer. Absorbance was measured at a wavelength of 490 nm. Data are expressed as percent viability relative to untreated control cells (set at 100%). Experiments were performed in triplicate and averaged.

Ex vivo studies in human specimens

Remnant de-identified specimens of human PDAC and adjacent normal pancreas were obtained following surgical resection and were immediately sliced with the Krumdieck tissue slicer.[17] Tissue slices 200 μM thick were plated in 12-well plates containing 50:50 Ham's/F12 and DMEM medium supplemented with 1% penicillin/streptomycin, 1% amphotericin B, 15% FBS, and 10 μg/mL dexamethasone. The average tissue weights were used to calculate the approximate cell number per tissue slice and infection was subsequently performed at 100 vp/cell. Infection media was replaced with fresh culture media 3 h p.i. At day 2, the total DNA was extracted from the slices using a QIAamp DNA Blood Mini kit. Viral copy number was quantitated by SYBR Green RT-PCR with adenoviral E4 primers and compensated with β-actin.[23,33]

Iodine-125 uptake

Human PDAC and adjacent normal pancreas tissues were seeded in 12-well plates and infected with 1 vp/cell. Culture media was aspirated

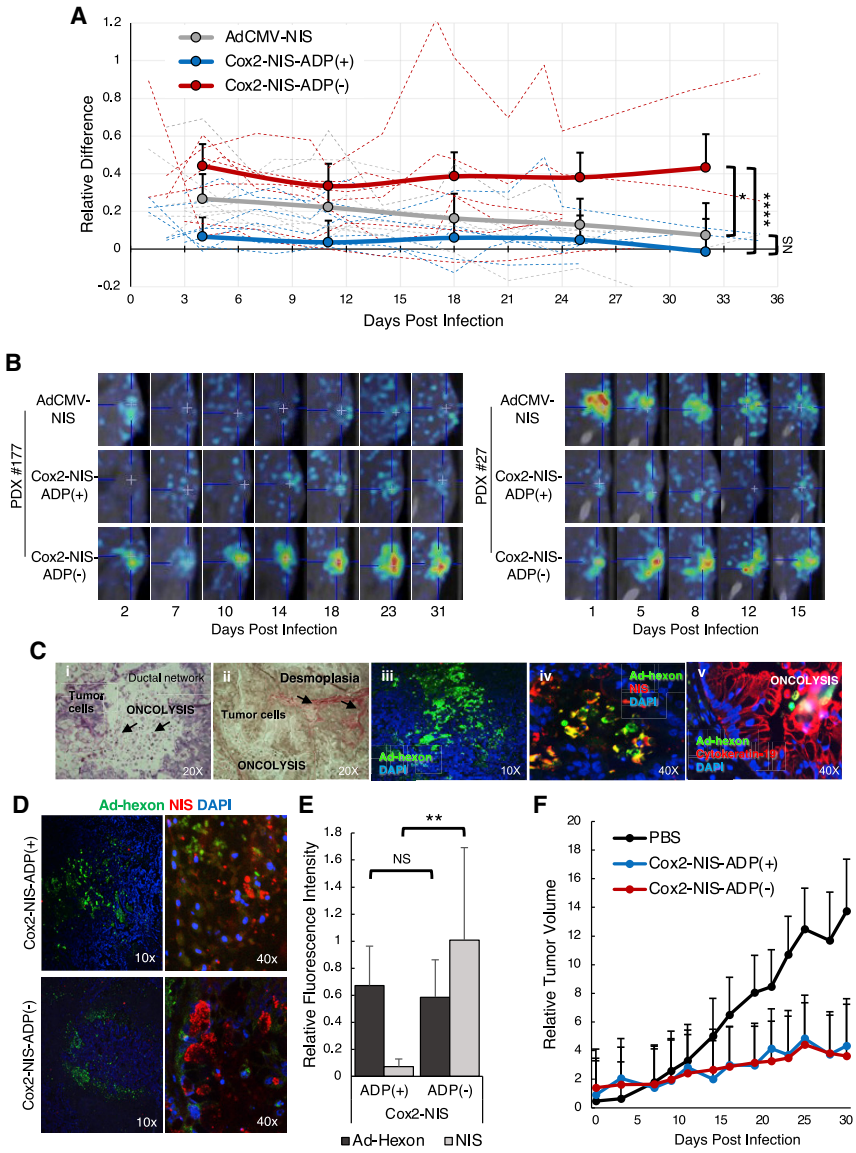

Figure 7. Radiotracer kinetics and tumor control in PDX

Biopsy-proven PDAC tissues from 6 different human patients were xenografted into groups of mice and injected with 4×10^{10} vp of either Ad-CMV-NIS, Cox2-NIS-ADP(+), Cox2-NIS-ADP(–), or PBS alone, resulting in each patient sample receiving all four treatment conditions. SPECT/CT imaging was performed with ^{99m}Tc. (A) Relative difference (RD) in uptake between tumor and muscle was calculated for each animal sample. Average RD of all mice/treatment group graphed in solid lines. Individual mouse RD displayed as dotted lines. Cox2-NIS-ADP(–) infected tumors showed significantly higher levels of radiotracer concentration compared to both Cox2-NIS-ADP(+) (*$p < 0.05$; ****$p < 0.0001$). (B) Representative images (including final image before mice euthanized) from 2 patient samples showed the improved signal and duration of imaging with Cox2-NIS-ADP(–). (C) Histology and immunofluorescent analyses of sequential slices of PDX tumor infected with Cox2-NIS-ADP(–): (i) H&E staining demonstrating oncolysis within the tumor; (ii) staining for collagen demonstrating desmoplastic nature of pancreatic tumor; (iii) immunostaining for Ad-hexon demonstrating active adenoviral infection in the tumor; (iv) immunostaining for Ad-hexon and NIS demonstrating NIS expression in tumor; (v) immunostaining for Ad-hexon and CK-19, a marker for pancreatic ductal cells demonstrating adenoviral infection and oncolysis in PDAC. (D) PDX tumor immunostaining for Ad-hexon protein and NIS. (E) Quantitative analysis of Ad-hexon and NIS staining using ImageJ software showed improved NIS expression after Cox2-NIS-ADP(–) infection (**$p < 0.01$; NS, not significant). (F) PDX growth curves. Both Cox2-NIS-ADP(+) and Cox2-NIS-ADP(–) slowed tumor growth compared to control ($p = 0.042$ and 0.039, respectively) but had no significant difference between the two viruses ($p = 0.996$). Error bars represent standard deviation.

2 days p.i. and replaced with 10 mM HEPES in HSBS containing 0.1 mM NaI. Control incubations included 0.1 mM KCLO4 (NIS inhibitor) to confirm NIS-specific radioiodine uptake. Cells were incubated for 45 min with 10^5 CPM of ^{125}I, followed by aspiration and rinsing in ice-cold Hank's balanced salt solution, then lysed in 1 M NaOH for 5 min with shaking. Radioactivity of lysates was measured using a gamma counter.[19]

Immunofluorescent analyses and histologic analysis

(1) Cell line preparation: cells were grown on chamber slides (50,000 per well), treated with 10 vp/cell in 100 µL of growth medium and incubated. Cells were washed in PBS, fixed (4% paraformaldehyde: 20 min; ice), and permeabilized (0.05% Triton X-100; 5 min; ice).

(2) Tissue preparation: PDAC Panc1 and PDX tumors were paraffin embedded, sectioned, and processed for antibody staining. Antigen retrieval was performed using a 1X universal antigen retrieval solution (R&D Systems, Minneapolis, MN, USA). Tissue sections were permeabilized (0.05% Triton X-100; 5 min; ice) and then incubated in a 5% BSA solution for 1 h at room temperature to reduce background.

(3) Immune staining: fixed and permeabilized cells and tissues were incubated on ice for 1 h (cells) or overnight (tissue) in a 5% (cells) or 2% (tissues) BSA solution containing combinations of the following primary antibodies at indicated dilution: anti-NIS (anti-FP5A, 1:500), anti-cytoskeleton associated protein (CYK4, 1:300), anti-cytokeratin-19 (RCK 108, 1:300), and anti-hexon-fluorescein isothiocyanate (FITC; AB1056, Millipore; 1:1,000). Cells and tissues were then incubated at room temperature for 30 min in 5% BSA (cells) or 1 h in 2% BSA (tissues) solutions containing Phycoerythrin (PE)-conjugated (1:1,000; red) and/or

FITC-conjugated (1:3,000; green) secondary antibodies. Cells and tissues were counterstained with a nuclear stain (DAPI) just prior to image capture using a fluorescent microscope. Plug-in functions of ImageJ software (NIH) were used to quantify NIS and hexon expression in tissues using RGB measure and normalized to DAPI.

(4) Histology: formalin-fixed, paraffin-embedded tissue sections were also stained with either H&E or picosirus red for collagen I and III. Images were captured by color bright-field microscopy.

Flow cytometry

Untreated or virus-treated cells (10 vp/cell for 3 h) were sub-cultured in growth medium, washed in PBS, fixed while maintaining a single-cell suspension (4% paraformaldehyde: 20 min; ice), and washed again in PBS before permeabilization (0.05% Triton X-100; 5 min; ice). Cells were incubated in a 5% BSA solution containing anti-NIS primary antibody (FP5A; 1:500) for 30 min on ice followed by PE-conjugated secondary antibody (1:1,000) and incubated for 30 min at room temperature. Cells were washed and re-suspended in PBS before analysis using a FacsCanto.

Non-invasive imaging and tumor control *in vivo* tumor models

To establish tumor models, we used: (1) pancreatic cancer Panc1 cells (2×10^6 per injection site); and (2) PDX derived from 6 human patients with biopsy-proven PDAC (Figure S1). The cells or tissues were inoculated subcutaneously into the right flank of female nude mice (6–8 weeks, Frederick Cancer Research). The tumor nodules were injected with a single virus dose when they reached a size of 8–10 mm in diameter (4×10^9 or 4×10^{10} vp/tumor in Panc1 models, and 4×10^{10} vp/tumor in PDX models; mixed with PBS for total volume of 50 μL). A high-resolution micro-SPECT/CT system was used for planar and fusion images as we described previously.[13] Briefly, 2 days p.i., and twice per week thereafter, mice received intraperitoneal injections of 0.5 mCi of sodium pertechnetate ($^{99m}TcO_4^-$), and SPECT/CT images were acquired 1 h later using a U-SPECT II scanner. Intratumoral radioisotope uptake was analyzed using PMOD Biomedical Image Quantification Software. Tumor volume was measured twice per week with calipers and was calculated as follows: tumor volume = (width2 × length)/2.

In vivo therapeutic studies in combination with radioactive iodine (^{131}I)

A549 cells (2.4×10^6) were injected subcutaneously into nude mice as we described above. Three groups received Ad monotherapy, three other groups received combination therapies (Ad plus ^{131}I), and two groups served as control (PBS alone and ^{131}I alone). Established xenografts (n = 8/group) at 6–8 mm in diameter were injected with 50 μL of either PBS or Ad at 4×10^{10} vp/tumor. Water for animals was supplemented with T4 (5 mg/L) 2 weeks prior to iodine administration and continued for the entire study. Low-iodine diet was prescribed to all animals 10 days before iodine administration and continued for 10 days after ^{131}I injection. 3 days p.i., 3.0 mCi of pharmaceutical grade ^{131}I (Cardinal Health, delivered in pre-dosed syringes) were injected intraperitoneally in the hood equipped with Hepa and charcoal filters. The dose range was calculated based on FDA recommended body surface area conversion to provide doses comparable to those in humans.[34] 11 and 19 days p.i. with Ad (8 and 16 days after ^{131}I administration), tumors and leg muscles were harvested and ^{131}I uptake was determined using a gamma counter. Virus-induced ^{131}I uptake was determined by first adjusting the ^{131}I uptake to tissue weight (CPM/mg) for tumors (n = 8) and then dividing by the corresponding CPM/mg for leg muscle of the same mouse. Tumor volume was calculated as described above. All animal studies were approved by institutional review boards and carried out in accordance with established animal care protocols.

Statistical analysis

Statistical analyses were done with R 3.4.4.[35] Differences in viral copy numbers between tumor and normal pancreatic tissues were evaluated using a general linear model. Analysis of iodine intake data was done using mixed models in R package lme4 with the viral construct treated as a fixed effect and the mouse as a random effect. The differences in dynamics of tumor growth between treatment groups were evaluated using repeated-measures analysis with R package nlme. The autoregressive correlation structure of the first order (corCAR1) was to account for correlation between adjustment time points. The viral constructs, week, and their interaction were treated as fixed effects and mouse as a random effect. The differences in oncolytic potential of OAd-NIS vectors were evaluated with general linear models using Day, Construct, and their interaction as predictors. For all analyses, pairwise comparisons between groups were done using R package emmeans with Tukey's adjustment. Remaining statistical analyses done with a two-tailed t test performed in Microsoft Excel. p values <0.05 were considered statistically significant.

SUPPLEMENTAL INFORMATION

Supplemental information can be found online at https://doi.org/10.1016/j.omto.2021.03.002.

ACKNOWLEDGMENTS

This study was supported by NIH NCI R01CA174861 (J.D. and M.E.F.-Z.); NIH NCI R01CA228760 (J.D.); NIH NCI P50CA101955 UAB-UMN Pancreatic Cancer SPORE Career Development Award (J.D.); University of Minnesota Masonic Cancer Center CRTI Translational Research Award grant (J.D. and M.G.R.); and Randy Shaver Cancer Research Grant (J.D. and M.G.R.). The authors thank Drs. John Morris (Mayo Clinic) and Lisa Koodie (UMN) for valuable discussions and technical support.

AUTHOR CONTRIBUTIONS

Conceptualization, J.D. and M.E.F.-Z.; methodology, B.B.E., E.I., and M.E.F.-Z.; investigation, M.G.R., B.B.E., E.I., E.J.T., K.J., and J.D.; resources, M.J.T.; formal analysis, E.I. and S.O.Z.; writing – original draft, M.G.R. and J.D.; writing – review & editing, M.G.R., C.J.L., M.E.F.-Z., and J.D.; funding acquisition, M.G.R., M.E.F.-Z., and J.D.; supervision, M.E.F.-Z. and J.D.

DECLARATION OF INTERESTS

The authors declare no competing interests.

REFERENCES

1. Miller, A., and Russell, S.J. (2016). The use of the NIS reporter gene for optimizing oncolytic virotherapy. Expert Opin. Biol. Ther. *16*, 15–32.
2. Touchefeu, Y., Franken, P., and Harrington, K.J. (2012). Radiovirotherapy: principles and prospects in oncology. Curr. Pharm. Des. *18*, 3313–3320.
3. Dwyer, R.M., Schatz, S.M., Bergert, E.R., Myers, R.M., Harvey, M.E., Classic, K.L., Blanco, M.C., Frisk, C.S., Marler, R.J., Davis, B.J., et al. (2005). A preclinical large animal model of adenovirus-mediated expression of the sodium-iodide symporter for radioiodide imaging and therapy of locally recurrent prostate cancer. Mol. Ther. *12*, 835–841.
4. Dingli, D., Peng, K.W., Harvey, M.E., Greipp, P.R., O'Connor, M.K., Cattaneo, R., Morris, J.C., and Russell, S.J. (2004). Image-guided radiovirotherapy for multiple myeloma using a recombinant measles virus expressing the thyroidal sodium iodide symporter. Blood *103*, 1641–1646.
5. Haddad, D., Chen, N.G., Zhang, Q., Chen, C.H., Yu, Y.A., Gonzalez, L., Carpenter, S.G., Carson, J., Au, J., Mittra, A., et al. (2011). Insertion of the human sodium iodide symporter to facilitate deep tissue imaging does not alter oncolytic or replication capability of a novel vaccinia virus. J. Transl. Med. *9*, 36.
6. Li, H., Nakashima, H., Decklever, T.D., Nace, R.A., and Russell, S.J. (2013). HSV-NIS, an oncolytic herpes simplex virus type 1 encoding human sodium iodide symporter for preclinical prostate cancer radiovirotherapy. Cancer Gene Ther. *20*, 478–485.
7. Naik, S., Nace, R., Federspiel, M.J., Barber, G.N., Peng, K.W., and Russell, S.J. (2012). Curative one-shot systemic virotherapy in murine myeloma. Leukemia *26*, 1870–1878.
8. Rajecki, M., Sarparanta, M., Hakkarainen, T., Tenhunen, M., Diaconu, I., Kuhmonen, V., Kairemo, K., Kanerva, A., Airaksinen, A.J., and Hemminki, A. (2012). SPECT/CT imaging of hNIS-expression after intravenous delivery of an oncolytic adenovirus and 131I. PLoS ONE *7*, e32871.
9. Spitzweg, C., Dietz, A.B., O'Connor, M.K., Bergert, E.R., Tindall, D.J., Young, C.Y., and Morris, J.C. (2001). In vivo sodium iodide symporter gene therapy of prostate cancer. Gene Ther. *8*, 1524–1531.
10. Warner, S.G., Kim, S.I., Chaurasiya, S., O'Leary, M.P., Lu, J., Sivanandam, V., Woo, Y., Chen, N.G., and Fong, Y. (2019). A Novel Chimeric Poxvirus Encoding hNIS Is Tumor-Tropic, Imageable, and Synergistic with Radioiodine to Sustain Colon Cancer Regression. Mol. Ther. Oncolytics *13*, 82–92.
11. Davydova, J., Gavrikova, T., Brown, E.J., Luo, X., Curiel, D.T., Vickers, S.M., and Yamamoto, M. (2010). In vivo bioimaging tracks conditionally replicative adenoviral replication and provides an early indication of viral antitumor efficacy. Cancer Sci. *101*, 474–481.
12. LaRocca, C.J., Han, J., Gavrikova, T., Armstrong, L., Oliveira, A.R., Shanley, R., Vickers, S.M., Yamamoto, M., and Davydova, J. (2015). Oncolytic adenovirus expressing interferon alpha in a syngeneic Syrian hamster model for the treatment of pancreatic cancer. Surgery *157*, 888–898.
13. Oneal, M.J., Trujillo, M.A., Davydova, J., McDonough, S., Yamamoto, M., and Morris, J.C., 3rd (2013). Effect of increased viral replication and infectivity enhancement on radioiodide uptake and oncolytic activity of adenovirus vectors expressing the sodium iodide symporter. Cancer Gene Ther. *20*, 195–200.
14. Oneal, M.J., Trujillo, M.A., Davydova, J., McDonough, S., Yamamoto, M., and Morris, J.C., 3rd (2012). Characterization of infectivity-enhanced conditionally replicating adenovectors for prostate cancer radiovirotherapy. Hum. Gene Ther. *23*, 951–959.
15. Ono, H.A., Le, L.P., Davydova, J.G., Gavrikova, T., and Yamamoto, M. (2005). Noninvasive visualization of adenovirus replication with a fluorescent reporter in the E3 region. Cancer Res. *65*, 10154–10158.
16. Salzwedel, A.O., Han, J., LaRocca, C.J., Shanley, R., Yamamoto, M., and Davydova, J. (2018). Combination of interferon-expressing oncolytic adenovirus with chemotherapy and radiation is highly synergistic in hamster model of pancreatic cancer. Oncotarget *9*, 18041–18052.
17. Armstrong, L., Arrington, A., Han, J., Gavrikova, T., Brown, E., Yamamoto, M., Vickers, S.M., and Davydova, J. (2012). Generation of a novel, cyclooxygenase-2-targeted, interferon-expressing, conditionally replicative adenovirus for pancreatic cancer therapy. Am. J. Surg. *204*, 741–750.
18. Armstrong, L., Davydova, J., Brown, E., Han, J., Yamamoto, M., and Vickers, S.M. (2012). Delivery of interferon alpha using a novel Cox2-controlled adenovirus for pancreatic cancer therapy. Surgery *152*, 114–122.
19. Trujillo, M.A., Oneal, M.J., Davydova, J., Bergert, E., Yamamoto, M., and Morris, J.C., 3rd (2009). Construction of an MUC-1 promoter driven, conditionally replicating adenovirus that expresses the sodium iodide symporter for gene therapy of breast cancer. Breast Cancer Res. *11*, R53.
20. Trujillo, M.A., Oneal, M.J., McDonough, S., Qin, R., and Morris, J.C. (2010). A probasin promoter, conditionally replicating adenovirus that expresses the sodium iodide symporter (NIS) for radiovirotherapy of prostate cancer. Gene Ther. *17*, 1325–1332.
21. Doronin, K., Toth, K., Kuppuswamy, M., Krajcsi, P., Tollefson, A.E., and Wold, W.S. (2003). Overexpression of the ADP (E3-11.6K) protein increases cell lysis and spread of adenovirus. Virology *305*, 378–387.
22. Tollefson, A.E., Scaria, A., Hermiston, T.W., Ryerse, J.S., Wold, L.J., and Wold, W.S. (1996). The adenovirus death protein (E3-11.6K) is required at very late stages of infection for efficient cell lysis and release of adenovirus from infected cells. J. Virol. *70*, 2296–2306.
23. Davydova, J., Le, L.P., Gavrikova, T., Wang, M., Krasnykh, V., and Yamamoto, M. (2004). Infectivity-enhanced cyclooxygenase-2-based conditionally replicative adenoviruses for esophageal adenocarcinoma treatment. Cancer Res. *64*, 4319–4327.
24. Ramírez, P.J., Vickers, S.M., Ono, H.A., Davydova, J., Takayama, K., Thompson, T.C., Curiel, D.T., Bland, K.I., and Yamamoto, M. (2008). Optimization of conditionally replicative adenovirus for pancreatic cancer and its evaluation in an orthotopic murine xenograft model. Am. J. Surg. *195*, 481–490.
25. Riesco-Eizaguirre, G., and Santisteban, P. (2006). A perspective view of sodium iodide symporter research and its clinical implications. Eur. J. Endocrinol. *155*, 495–512.
26. Barton, K.N., Stricker, H., Brown, S.L., Elshaikh, M., Aref, I., Lu, M., Pegg, J., Zhang, Y., Karvelis, K.C., Siddiqui, F., et al. (2008). Phase I study of noninvasive imaging of adenovirus-mediated gene expression in the human prostate. Mol. Ther. *16*, 1761–1769.
27. Galanis, E., Atherton, P.J., Maurer, M.J., Knutson, K.L., Dowdy, S.C., Cliby, W.A., Haluska, P., Jr., Long, H.J., Oberg, A., Aderca, I., et al. (2015). Oncolytic measles virus expressing the sodium iodide symporter to treat drug-resistant ovarian cancer. Cancer Res. *75*, 22–30.
28. Rajecki, M., Kangasmäki, A., Laasonen, L., Escutenaire, S., Hakkarainen, T., Haukka, J., Ristimäki, A., Kairemo, K., Kangasniemi, L., Kiljunen, T., et al. (2011). Sodium iodide symporter SPECT imaging of a patient treated with oncolytic adenovirus Ad5/3-Δ24-hNIS. Mol. Ther. *19*, 629–631.
29. Russell, S.J., Federspiel, M.J., Peng, K.W., Tong, C., Dingli, D., Morice, W.G., Lowe, V., O'Connor, M.K., Kyle, R.A., Leung, N., et al. (2014). Remission of disseminated cancer after systemic oncolytic virotherapy. Mayo Clin. Proc. *89*, 926–933.
30. Kimbrough, C.W., Khanal, A., Zeiderman, M., Khanal, B.R., Burton, N.C., McMasters, K.M., Vickers, S.M., Grizzle, W.E., and McNally, L.R. (2015). Targeting Acidity in Pancreatic Adenocarcinoma: Multispectral Optoacoustic Tomography Detects pH-Low Insertion Peptide Probes In Vivo. Clin. Cancer Res. *21*, 4576–4585.
31. DeRosier, L.C., Huang, Z.Q., Sellers, J.C., Buchsbaum, D.J., and Vickers, S.M. (2006). Treatment with gemcitabine and TRA-8 anti-death receptor-5 mAb reduces pancreatic adenocarcinoma cell viability in vitro and growth in vivo. J. Gastrointest. Surg. *10*, 1291–1300, discussion 1300.
32. Davydova, J., and Yamamoto, M. (2013). Oncolytic adenoviruses: design, generation, and experimental procedures. Curr. Protoc. Hum. Genet. *Chapter 12*. Unit 12.14.
33. Koodie, L., Robertson, M.G., Chandrashekar, M., Ruth, G., Dunning, M., Bianco, R.W., and Davydova, J. (2019). Rodents Versus Pig Model for Assessing the Performance of Serotype Chimeric Ad5/3 Oncolytic Adenoviruses. Cancers (Basel) *11*, 189.
34. Trujillo, M.A., Oneal, M.J., McDonough, S., Qin, R., and Morris, J.C. (2012). A steep radioiodine dose response scalable to humans in sodium-iodide symporter (NIS)-mediated radiovirotherapy for prostate cancer. Cancer Gene Ther. *19*, 839–844.
35. R Development Core Team. (2013). R: A language and environment for statistical computing (R Foundation for Statistical Computing).